Environ. Sci. Technol. **2005**, *39,* 4990−4995

Nitrogen and Carbon Dioxide Adsorption by Soils

PETER I. RAVIKOVITCH,*,† BILL W. BOGAN,‡ AND ALEXANDER V. NEIMARK†

TRI/Princeton, 601 Prospect Avenue, Princeton, New Jersey 08542, and Gas Technology Institute, 1700 South Mount Prospect Road, Des Plaines, Illinois 60018

High-resolution nitrogen (77 K) and carbon dioxide (273 K) adsorption at subatmospheric pressures has been studied for a range of model soils of various origins with different organic matter (OM) contents. It is demonstrated that N_2 and CO_2 molecules probe different regions of soil particles. Nitrogen is adsorbed primarily on the outer surface of soil particles, while CO_2 has a higher affinity to OM domains. Low-pressure nitrogen adsorption reveals that soil particle surfaces consist of clay/mineral domains with discrete patches of OM. A linear correlation has been found between the CO_2 uptake and the amount of organic carbon reduced per unit of the external surface area. A new method for discriminating the microporosity of soil particles and accessibility of OM has been proposed.

Introduction

Reduced availability of organic contaminants to chemical or biological treatment is usually attributed to sequestration in soil particles, especially in soil organic matter (OM) (*1*−*3*). Recent efforts to correlate soil properties with reduced availability of chemicals identified several contributing factors, such as the organic carbon (OC) content and surface area (*4*), humin content of OM (*5*), nanoporosity (*6*), black carbon fractions (*7*−*10*), loosely bound humic substances and humin (*11*), and extent of the humic/fulvic acid overlayer (*12*). Despite an abundance of diverse experimental studies, the physicochemical mechanisms of limited bioavailability and the role of humic substances are not well understood.

One of the challenges is the characterization of the distribution of OM within the aggregates of soil particles. In our previous paper (*12*), we introduced a new parameter termed the "humic coverage index" (HCI). HCI is the amount of humic acid and fulvic acid (HA and FA) per unit of external area of soil particles. HCI has been suggested as a determining factor characterizing the extent of organic coverage. It was found in biodegradation experiments performed for a range of model soils with different amounts of OM that each bacterial strain displayed maximal contaminant biodegradation at a particular value of HCI, and that the extent of biodegradation decreased as HCI increased or decreased from this "optimal" value; the specific optimal HCI value for contaminant biodegradation varied for different bacterial strains. Moreover, it was shown that fulvic acid supplementation enhances biodegradation when the soil in question is below the optimal HCI for the relevant degrader strain, but has no such effect if the soil is at or above the strain's optimal HCI.

The purpose of the present work is to obtain a better understanding of the link between the physical properties of soils and the results of previous biodegradation experiments (*12*). We use a combination of high-resolution (low-pressure) nitrogen and carbon dioxide adsorption techniques to characterize heterogeneity of soil surfaces and soil porosity and obtain information on the distribution of OM within soil aggregates. We demonstrate a clear quantitative correlation between the results obtained by N_2 and CO_2. It is shown that N_2 and CO_2 probe different domains of soil structure and, thus, complement each other.

Materials and Methods

Soils. Collection and Characterization. Eleven model soils were collected from noncontaminated grassy or wooded areas (soils 1−6) and construction sites (soils 7−10 and 12) in the Northwestern Greater Chicago area. Soil 11 was a commercially available potting soil. Total organic carbon (TOC) contents of the soils were measured by ashing soil samples at 440 °C, as per ASTM method D2974-87. Soil organic matter was fractionated into HAs, FAs, and humin as previously reported (*13*). In brief, soil samples were extracted twice with 0.1 M NaOH; the supernatants were combined and acidified to precipitate HA, while the supernatant (FA) was run through an XAD8 column for desalting purposes. The humin fraction was acid (HCl)-washed, and rinsed with water until the rinsate contained no Cl^-, at which point it was dried at 60 °C. Solid fractions (humic acid and humin) were measured using a Shimadzu TOC-V/SSM-5000A analyzer; aqueous fulvic acid samples were determined using a Shimadzu TOC-500 analyzer.

High-Resolution Nitrogen Adsorption. High-resolution nitrogen adsorption/desorption isotherms were measured at the normal boiling temperature (77.4 K) using an Autosorb-1C automated volumetric instrument from Quantachrome Instruments equipped with a 0.0001−1 Torr pressure transducer. Before the measurements, the soil samples were vacuum-degassed at temperatures not exceeding 120 °C for a period of ca. 24 h. Determination of the void volume was performed by helium using standard procedures. Low-pressure data points were corrected on the thermal transpiration effect according to standard procedures.

CO_2 Sorption. CO_2 sorption/desorption isotherms were measured at 273 K. The saturation vapor pressure of CO_2 at 273 K was taken as 26142 Torr. A homemade electric thermostat was used to maintain the temperature within ±0.2 K. All the samples were measured using the same experimental protocol. A total of 52 adsorption points were collected in the interval of relative pressures from $p/p_0 = 1 \times 10^{-5}$ to $p/p_0 = 0.029$ followed by 30 desorption points. The pressure point was acquired after the pressure reading had changed by less than 3 Torr (less than 0.03 Torr in the range of $p/p_0 < 3 \times 10^{-3}$) for a time period of 5 min.

Results and Discussion

Soil Characteristics. Relevant characteristics (i.e., TOC content, levels of humic and fulvic acids, particle size distribution, and textural classification) of the 12 soils included in this study are given in Table 1. The organic carbon content of the soils ranged from a low of slightly over 2% by mass (soils 1 and 8), to a high of over 27% (the commercial potting soil, soil 11). As would be expected, this soil and the six that were obtained from vegetated (grassy and wooded)

* Corresponding author phone: (609) 430-4830; fax: (609) 683-7149; e-mail: ravikovi@triprinceton.org.
† TRI/Princeton.
‡ Gas Technology Institute.

10.1021/es048307b CCC: $30.25
© 2005 American Chemical Society
Published on Web 05/19/2005

TABLE 1. TOC, HA, and FA Contents (%) (As Determined from SOM Fractionations) and Sand, Silt, and Clay Contents (%) for Each Soil

soil	TOC[a]	HA[a]	FA[a]	sand	silt	clay	textural classification
1	2.32	0.14	0.01	25.4	51.1	27.5	clay loam/loam
2	5.78	0.71	0.05	64.0	25.3	10.7	sandy loam
3	11.20	2.18	0.16	70.8	18.1	11.1	sandy loam
4	24.30	3.13	0.97	73.5	10.6	15.9	sandy loam
5	3.58	0.23	0.03	40.6	33.0	26.4	loam
6	9.13	1.69	0.10	51.8	26.3	21.9	sandy clay loam
7	5.95	0.05	0.03	44.5	19.4	36.1	sandy clay
8	2.22	0.02	<0.01	22.7	41.5	35.8	clay loam
9	2.89	0.01	0.01	35.2	23.3	41.5	clay
10	3.92	0.03	0.04	35.0	29.2	35.8	clay loam
11	27.40	3.73	0.25	42.4	36.2	21.4	loam
12	4.22	0.08	0.03	47.2	23.2	29.6	sandy clay loam

[a] Expressed as a mass percentage of the whole soil.

areas (soils 1−6) were, in general, higher in TOC than those which were collected from construction sites. Also, in this latter group of soils (7−10 and 12), the overwhelming majority of OM which was present was in the form of humin; this is in contrast to the recently vegetated soils, which, in general, all contained considerably higher amounts of humic and/or fulvic acids. Considerable differences were observed in the sand/silt/clay particle size distribution between the soils, as is shown in Table 1.

Nitrogen Adsorption. Nitrogen adsorption isotherms (see Supporting Information Figure S1) exhibit H3-type hysteresis loops, according to IUPAC classification (*14*), which are typical for materials with lamellar structures, e.g., clays. The hysteresis loops close in the relative pressure range between ca. $P/P_0 = 0.44$ and $P/P_0 = 0.48$, which is within a typical range for the lower limit of the N_2 hysteresis loop (*14*). It is well-known that the step on the desorption branch occurring at the lower closure point of the hysteresis loop does not indicate the presence of ∼4 nm mesopores (pores that empty at $P/P_0 \approx 0.4$ according to the cylindrical pore model). It is likely that such steps indicate desorption by cavitation from mesopores larger than ∼4 nm, which were blocked by narrower pores (*15*). This mechanism of desorption is consistent with various models for the interlayer porosity in clays (*16*). The height of the step on the desorption branch may be regarded as a measure of the amount of mesopores which were blocked. However, there is no correlation between the height of the step and either the OC or clay content of the soils.

Specific surface areas were calculated from the BET method applied in the region of relative pressures from $p/p_0 = 0.05$ to $p/p_0 = 0.3$ (*14*). Surface areas and corresponding BET *C* constants are listed in Table 2. The BET specific surface areas can be considered as estimates of the surface area contributed by the overlayer of HA and FA, plus any exposed surface of humin/mineral core particles.

The samples studied had different extents of OM coverage, which is quantified as a humic coverage index (HCI) and is listed in Table 2. This number is derived from the summed HA and FA contents of the soil (expressed on a mass basis), divided by the BET surface area. The resultant quantity, with units of mg/m^2, provides an expression of how much HA + FA coats the surfaces of the core soil particles. HCI can be conceptualized as combining the extent and thickness of the humic/fulvic acid overlayer. In addition, Table 2 also lists total organic carbon content per unit of BET surface area. These latter numbers correlate with HCI. The specific surface areas decrease with an increase in the organic matter content of soils.

TABLE 2. BET Specific Surface Areas and Energetic *C* Constants, As Measured by N_2 Adsorption Isotherms, and Maximum CO_2 Uptake at ∼1 atm per Unit of N_2 BET Surface Area

soil	BET surface area, S_{N^2} (m^2/g)	BET *C* constant	OM fractional coverage, α	HCI[a] (mg/m^2)	OC per area[a] (mg/m^2)	CO_2 max uptake (mg/m^2)
1	30.3	95	0.12	0.050	0.77	0.14
2	24.5	126	0	0.310	2.36	0.24
3	4.92	43	0.57	4.756	22.7	1.18
4	3.03	22	1.00	13.53	80.1	2.61
5	23.2	72	0.15	0.112	1.55	0.20
6	15.4	51	0.35	1.162	5.93	0.47
7	25.2	114	0.01	0.031	2.36	0.22
8	29.5	79	0.15	0.008	0.75	0.13
9	28.0	97	0.08	0.005	1.03	0.15
10	25.1	81	0.14	0.029	1.56	0.17
11	16.5	56	0.33	2.403	16.6	0.61
12	19.4	75	0.16	0.057	2.17	0.23

[a] HCI is the humic coverage index, and "OC per area" is the total OC content per unit of N_2 BET surface area.

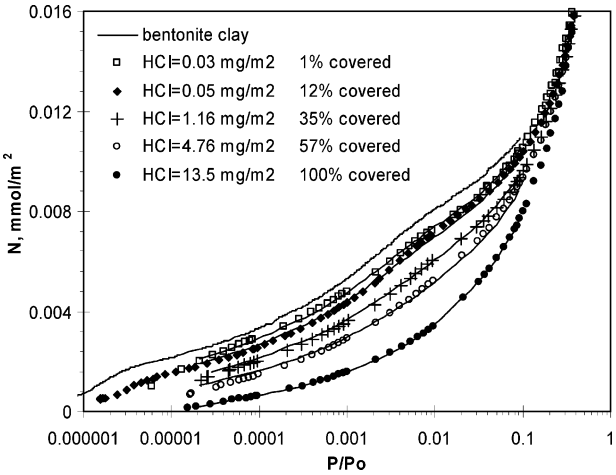

FIGURE 1. Reduced high-resolution N_2 adsorption isotherms on soils with different HCIs. Lines are fits with eq 1 obtained by using soils 2 and 4 as references for the bare mineral and OM-covered surfaces, respectively. The isotherm on a Na-bentonite clay (*17*) is shown for comparison only.

High-resolution adsorption is a more sensitive method to study energetics of gas adsorption than the standard BET method, which is limited to the range of relative pressures above ca. $p/p_0 = 0.05$. Figure 1 shows the low-pressure portions of N_2 isotherms at 77 K normalized on the BET specific surface areas. The isotherms coincide at the relative pressure of ca. $p/p_0 = 0.4$, after the monolayer adsorption is completed. In the low-pressure region, however, adsorption isotherms for soils with different organic coverages show important differences. For soils with a low OM coverage, the adsorption isotherms are similar to the isotherms on clays. Figure 1 also includes an isotherm on Na-bentonite clay taken from the literature (*17*). The adsorption per unit area decreases as the extent of humic coverage increases, and therefore, the energy of gas−solid interactions decreases (*18*).

Adsorption potential distributions (APDs) provide important information about the energetics of gas adsorption. APDs were calculated as the derivative of the isotherm with respect to the so-called adsorption potential (*19*), i.e., $\mathrm{d}(v/v_m)/\mathrm{d}A$, where v/v_m is the reduced N_2 adsorption in number of monolayers, and $A = -RT\ln(p/p_0)$. The derivatives were calculated using a forward difference scheme. Within the APD approximation, the derivative of the isotherm indicates the distribution of sites with different adsorption energies.

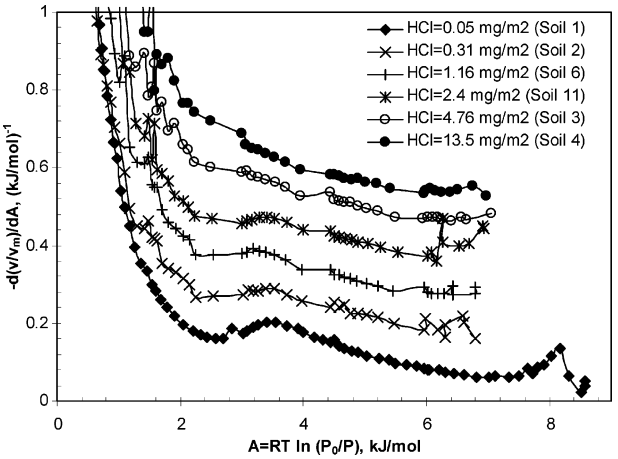

FIGURE 2. Selected adsorption potential distributions determined from nitrogen adsorption isotherms. The vertical scale is shifted for soils 2, 6, 11, 3, and 4 by 0.1, 0.2, 0.3, 0.4, and 0.5 (kJ/mol)$^{-1}$, respectively.

With respect to N_2 adsorption, OM presents a low-energy surface which is distinguishable from high-energy clay mineral surfaces. APDs for soils with low OM coverage exhibit a peak at $A = 3-4$ kJ/mol (Figure 2). A similar peak (not shown) is observed for the reference Na-bentonite clay and also for other clays, and may be identified as the monolayer adsorption on the clay basal plane (*20*). The presence of this peak in the APD of soils can be explained considering that clays make a dominant contribution to the surface area as compared to most other minerals in soils. This fact is known for marine sediments (*18*). As the amount of soil OM per surface area increases, the monolayer adsorption peak gradually diminishes; the distribution of site energies becomes broader, which can be explained by partial coverage of mineral surfaces. The peak completely disappears for the soil with the highest OM coverage (soil 4, HCI $\approx$ 13.2 mg/m^2). The presence of the monolayer adsorption peak for soils with intermediate OM coverages strongly supports the picture of a nonuniform, patchy overlayer of OM covering the external surface of soil particles. It is also consistent with the fact that OM accumulates first at the edge sites of clay minerals (*18*), which still leaves bare basal planes available for N_2 adsorption.

It is of interest to compare the APD results with a simple model that assumes a homogeneous OM coverage of soil particles. Assuming spherical particles and a 1 g/cm^3 density for the OM overlayer, the amount of OM required for a *uniform* monolayer coverage is estimated to be $\sim$1 mg/m^2, or $\sim$1 nm equivalent thickness. It follows, however, from APDs (Figure 2) that the monolayer adsorption peak at the same position as for bare clays is recognizable even for soils with OM coverage as high as 20 mg/m^2 (HCI = 4.76 mg/m^2). This indicates that the OM coating of soil particles occurs in the form of discrete patches rather than a uniform layer. Only soils with a higher amount of OM per unit area are likely to be covered by an extensive humic layer, sufficient to coat the core particle mineral surfaces.

The above picture suggests an efficient method for quantifying the fractional OM coverage of soils based on low-pressure N_2 adsorption isotherms. Adsorption isotherms on soils can be described very well as a superposition of the isotherm on a bare mineral surface and the isotherm on soil with the highest and, presumably, uniform OM coverage per unit area:

$$N = \alpha N_{\mathrm{OM}} + (1 - \alpha) N_{\mathrm{bare}} \qquad (1)$$

where N_{bare} is the adsorption per unit area on a reference bare mineral surface, N_{OM} is the adsorption on an OM-covered surface, and α is the *fractional OM coverage*. The method depends on the choice of the reference isotherms. Here we assume that the soil with the highest OM content per unit area and the highest HCI is fully coated by an organic overlayer (soil 4). The isotherm is given in tabulated form in Table S1 (see the Supporting Information). The choice of the reference isotherm on a bare mineral surface is less obvious. If we take adsorption on the bentonite clay surface as a reference, the fractional coverage will likely be overestimated because this clay exhibits somewhat higher adsorption per unit area than the soil samples (Figure 1). An ideal reference surface would be the soil under study after removal of OM. This option will be explored in future studies. In this work, we chose the isotherm on soil 2 as a reference for the bare mineral surface as it exhibits the highest adsorption per unit area in the low-pressure range, and the highest BET C constant. Thus, using eq 1 and soils 2 and 4 as the two references, we have fitted isotherms on other soils in the relative pressure range below $p/p_0 = 0.1$. The results are shown in Figure 1 and in Table 2. It is seen that the simple model of eq 1 works very well and allows one to calculate the fractional coverage.

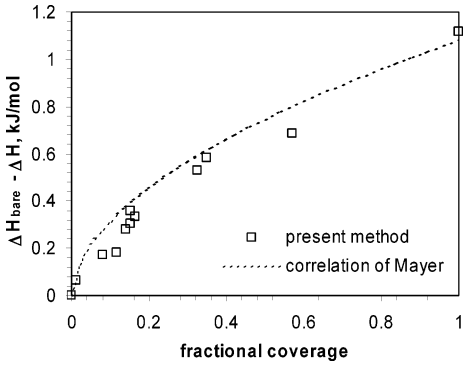

FIGURE 3. Difference in the net heat of N_2 adsorption between the bare and OM-covered soil surfaces as a function of the fractional OM coverage. The correlation from ref *18* is also shown.

In Figure 3 we plot the relationship between the difference in the net heat of N_2 adsorption on the bare mineral and OM-covered soil surfaces, $\Delta H_{\mathrm{bare}} - \Delta H$, as a function of the fractional OM coverage. The heats of adsorption were calculated from the BET theory as $\Delta H = RT \ln C$. Again, we used soil 2 as a reference to calculate ΔH_{bare}. It follows that the difference $\Delta H_{\mathrm{bare}} - \Delta H$ increases as the OM coverage increases. Our results are in surprisingly good agreement with the correlation found by Myers (*18*), who used a completely different method. Myers used adsorption of organic compounds, such as adipic and fatty acids, on alumina, silica, and oxidized marine sediments, and calculated fractional coverage from molecular dimensions and molar adsorption. (Note that the correlation presented in the original paper (*18*) should be multiplied by 77.4/299 (*21*).) The comparison is in favor of the present method, as it does not require the removal of OM from soils and measurement of two isotherms, before and after the removal. However, for a more detailed study, one should measure low-pressure adsorption both before and after the removal of OM.

Our results are in general agreement with density fractionation and X-ray photoelectron spectroscopy (XPS) characterization of organic matter in marine sediments (*22*). These methods showed that OM is located in discrete spots on the surface and decreases in thickness as the amount of OC per unit area decreases. XPS shows quite substantial carbon content by mass ($\sim$10 wt %) even for soils with a low area-normalized OC content (below $\sim$3 mg/m^2) (see Figure 9 in ref *22*). This is in broad agreement with our results (see Figure S2 in the Supporting Information), which show a fractional

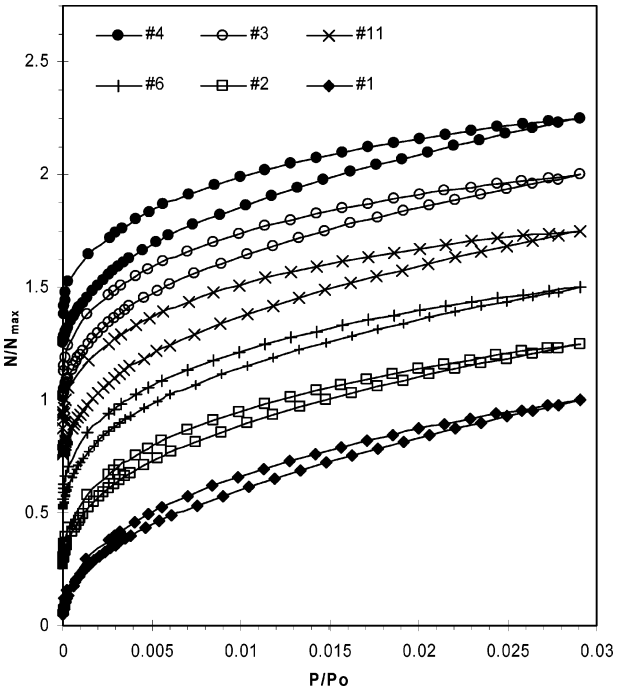

FIGURE 4. Carbon dioxide sorption/desorption isotherms at 273 K normalized on the maximum uptake at $p/p_0 = 0.029$ (~1 atm). The vertical scale is shifted by 0.25, 0.5, 0.75, 1, and 1.25 for soils 2, 6, 11, 3, and 4, respectively.

OM coverage of ~0.1 for soils with a low OC content. It should be noted, however, that the results in this region are sensitive to the choice of the reference isotherm on a bare mineral surface.

Carbon Dioxide Sorption. CO_2 sorption/desorption isotherms are shown in Figure 4. The isotherms are nonlinear and exhibit moderate hysteresis loops. The extent of the hysteresis loops tends to increase with an increase in TOC content (Table 1). Similar or even much larger hysteresis loops for CO_2 sorption were reported for other soils, especially ones with a high OM content, and also for peat and its purified fractions, humic acid and humin (*23*).

It is difficult to define an unambiguous model to interpret CO_2 sorption data in quantitative terms. It is known that CO_2 adsorption at 273 K and subatmospheric pressures can fill micropores that are only a few molecular diameters of the adsorbate molecule. This is supported by the molecular modeling of CO_2 in slit-shaped micropores with graphitic walls (*24*, *25*). The isotherms in micropores are nonlinear and exhibit micropore-filling swings which shift to higher relative pressures as the pore size increases (see, e.g., Figure 3c,d in ref *25*). As a reference, for example, the CO_2 adsorption isotherm on a homogeneous graphite surface at subatmospheric pressures is practically linear. Also, CO_2 dissolves in amorphous regions of OM, and this absorption/dissolution phenomenon is expected to produce a linear sorption isotherm.

Interpretation of carbon dioxide adsorption to soils has been somewhat controversial (*8*, *26*−*28*). It is often assumed that very narrow micropores are not accessible to N_2 within reasonable equilibration times (*14*). Thus, the surface areas obtained from N_2 are the surface areas contributed mainly by the overlayer of HA and FA as well as any exposed surface of the core humin/mineral soil particles (*12*). This assumption is justified because at low temperatures of standard N_2 adsorption measurements (77 K) diffusion into subnanometer pores and across the organic interfaces may be strongly activated (*26*). Therefore, N_2 at 77 K cannot penetrate into narrow micropores, especially those which are "buried" by the overlayer of HA and FA. Carbon dioxide adsorption at ambient temperatures has been proposed as an alternative to N_2 adsorption to characterize nanoporosity in soils (*3*, *23*, *26*). The nonlinear shape of CO_2 isotherms may be associated with adsorption in micropores and with strong adsorption on high-energy sites due to interactions of CO_2 with mineral and OM fractions of soils. The fact that the shape of the isotherms is not very different for soils with very high (e.g., soil 11) and very low (e.g., soil 1) amounts of OM indicates that nonlinearity is not likely to be associated with CO_2 adsorption/absorption on OM (Figure 4). On the other hand, highly nonlinear CO_2 isotherms were reported for soils with a very high OM content, such as peat (*23*, *26*). The latter fact is difficult to explain without invoking the concept of micropore filling. It was proposed that micropores may exist in glassy regions of OM (*29*) or in the high surface area black carbon fractions of soils (*8*).

The following analysis suggests that, in our case, the nonlinear shape of CO_2 isotherms is more likely to be associated with interactions of CO_2 with high-energy adsorption sites on mineral surfaces. The isotherms for different soils can be superimposed on one another by scaling them on the maximum CO_2 uptake at $p/p_0 = 0.029$. In this case, the differences between CO_2 isotherms for soils with various OM contents are seen only at low pressures. The adsorption branches for soils with a higher amount of OM deviate downward, while the corresponding desorption branches deviate upward. In other words, the increase in OM content leads to a larger extent of the hysteresis loop, as seen in Figure 4. The hysteresis in this case can be explained as a purely kinetic phenomenon caused by slow diffusion of CO_2 into OM domains. This follows from the fact that the experimental time to reach the maximum CO_2 uptake at $p/p_0 = 0.029$ strongly correlates with the OM coverage per unit area. In other words, the larger the OM coverage, the longer it takes to reach (quasi)equilibrium for a given experimental protocol (see Figure S3 in the Supporting Information). This type of hysteresis can be described quantitatively using the diffusion-controlled hysteresis (DCH) model, which couples the diffusion equation with a generally nonlinear sorption term, and allows one to estimate the equilibrium sorption isotherm from nonequilibrium sorption/desorption measurements (*30*). Detailed discussion of the CO_2 hysteresis is beyond the scope of the present paper. Based on experience with other materials for which CO_2 exhibits similar extents of the sorption/desorption hysteresis loop, the equilibrium isotherm is close to the average between the adsorption and desorption branches, and the maximum CO_2 uptake is close to the equilibrium one (*30*).

Given uncertainties in the interpretation of CO_2 uptake by soils, we are not in the position to choose a particular sorption model. Micropore filling is usually described using the empirical Dubinin−Radushkevitch equation (*14*). A more rigorous description of micropore filling is based on molecular models such as nonlocal density functional theory and Monte Carlo simulations (*25*). However, these advanced approaches require a good molecular model of soil, which is lacking. For example, the surface areas of soils could be calculated from the self-consistent method using molecular models of N_2 and CO_2 adsorption in carbonaceous slit pores (*25*). However, this model is not fully justified for soils. For any model, however, the obtained pore volume or surface area would be proportional to the maximum CO_2 uptake. We, therefore, choose the maximum CO_2 uptake at ~1 atm ($p/p_0 = 0.029$) as a characteristic point on CO_2 sorption isotherms.

Figure 5 shows a relationship between the maximum CO_2 uptake and the total organic carbon content; both quantities were reduced on the corresponding N_2 BET surface areas. It is seen that, as the amount of organic carbon per unit area of soil increases, so does the CO_2 uptake. At the same time,

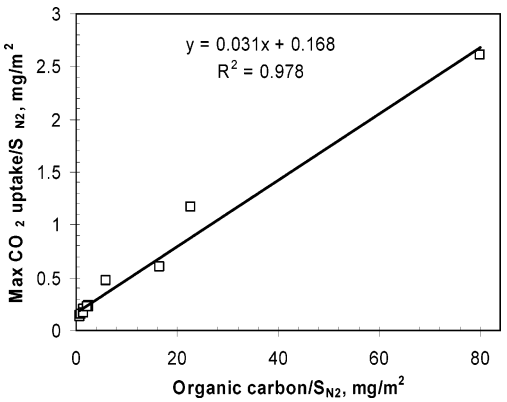

FIGURE 5. Relationship between CO_2 uptake and the organic carbon content per unit of N_2 BET surface area.

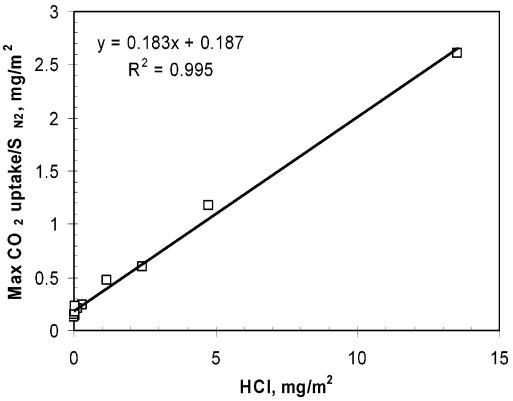

FIGURE 6. Relationship between CO_2 uptake per unit area and the humic coverage index.

the N_2 BET surface area decreases as the OC content increases. This means that N_2 and CO_2 probe different regions of the soil matrix. N_2 is adsorbed primarily on the outer surface of soil particles, while CO_2 has a high affinity for OM and, possibly, microporous regions of soils. The correlation in Figure 5 is practically linear ($R^2 = 0.978$). The slope of the linear regression line gives ~3.1 wt % CO_2 per unit weight of total organic carbon, which is in reasonable agreement with those from other studies, for example, CO_2 uptake by peat (*23, 26*). The intercept indicates CO_2 adsorption on mineral surfaces for soils with negligibly small OM coverage.

A similar linear relationship is observed when the maximum CO_2 uptake is plotted against the HCl index (Figure 6). The data show excellent linear correlation ($R^2 = 0.995$). The fact that HCl correlates better with maximum CO_2 uptake than does area-normalized TOC implies a difference in the gas-uptake behavior of HA and FA vs "bulk" OC; the one datapoint which points this out is the "potting soil" (soil 11), which has much less HA/FA per unit area than one would expect on the basis of its TOC content (see Table 2). This datapoint shows a better fit with the regression line in Figure 6 than with that in Figure 5.

The linear correlation between CO_2 uptake and OC content per unit area (Figure 5) suggests a method for determining the accessibility of OM in soils and the presence of micropores. We assume that the slope of the linear regression line in Figure 5 gives an *average* partitioning coefficient of CO_2 in soil OM (as it is reasonable to assume given the fact that we obtained ~0.03 g/g for a range of different soils) and that the CO_2 data are sufficiently close to equilibrium. In this case, if the data point falls appreciably above the linear regression line, this might indicate increased CO_2 uptake due to, most likely, the presence of micropores or other high-energy sites, inaccessible to N_2 molecules, but accessible to CO_2. At the same time, if the point falls below the regression line, this might indicate limited accessibility of OM to CO_2 sorption. This hypothesis is currently being tested.

Acknowledgments

This work was supported by the USDA (Grant 2001-35107-1053 to TRI/Princeton), DOE (Research Contract No. DE-AC26-99BC15223 to Gas Technology Institute), and Gas Research Institute. We thank James Rice (South Dakota State University) for fractionation and quantitation of humic materials.

Supporting Information Available

N_2 adsorption isotherms (Figure S1), relationship between the fractional OM coverage and OC content (Figure S2), correlation between the CO_2 sorption time and OC content (Figure S3), and tabular data for the reference isotherm on OM-covered soil. This material is available free of charge via the Internet at http://pubs.acs.org.

Literature Cited

(1) Luthy, R.; Aiken, G.; Brusseau, M.; Cunningham, S.; Gschwend, P.; Pignatello, J.; Reinhard, M.; Traina, S.; Weber, W.; Westall, J. Sequestration of Hydrophobic Organic Contaminants by Geosorbents. *J. Environ. Sci. Technol.* **1997**, *31*, 3341−3347.

(2) Weber, W. J.; Huang, W. L. A distributed reactivity model for sorption by soils and sediments.4. Intraparticle heterogeneity and phase- distribution relationships under nonequilibrium conditions. *Environ. Sci. Technol.* **1996**, *30*, 881−888.

(3) Xing, B. S.; Pignatello, J. J. Dual-mode sorption of low-polarity compounds in glassy poly(vinyl chloride) and soil organic matter. *Environ. Sci. Technol.* **1997**, *31*, 792−799.

(4) Chung, N.; Alexander, M. Effect of soil properties on bioavailability and extractability of phenanthrene and atrazine sequestered in soil. *Chemosphere* **2002**, *48*, 109−115.

(5) White, J. C.; Hunter, M.; Nam, K. P.; Pignatello, J. J.; Alexander, M. Correlation between biological and physical availabilities of phenanthrene in soils and soil humin in aging experiments. *Environ. Toxicol. Chem.* **1999**, *18*, 1720−1727.

(6) Nam, K.; Alexander, M. Role of nanoporosity and hydrophobicity in sequestration and bioavailability: Tests with model solids. *Environ. Sci. Technol.* **1998**, *32*, 71−74.

(7) Gustafsson, O.; Haghseta, F.; Chan, C.; MacFarlane, J.; Gschwend, P. M. Quantification of the dilute sedimentary soot phase: Implications for PAH speciation and bioavailability. *Environ. Sci. Technol.* **1997**, *31*, 203−209.

(8) Chiou, C. T.; Kile, D. E.; Rutherford, D. W.; Sheng, G. Y.; Boyd, S. A. Sorption of selected organic compounds from water to a peat soil and its humic-acid and humin fractions: Potential sources of the sorption nonlinearity. *Environ. Sci. Technol.* **2000**, *34*, 1254−1258.

(9) Song, J. Z.; Peng, P. A.; Huang, W. L. Black carbon and kerogen in soils and sediments. 1. Quantification and characterization. *Environ. Sci. Technol.* **2002**, *36*, 3960−3967.

(10) Accardi-Dey, A.; Gschwend, P. M. Assessing the combined roles of natural organic matter and black carbon as sorbents in sediments. *Environ. Sci. Technol.* **2002**, *36*, 21−29.

(11) Nam, K.; Kim, J. Y. Role of loosely bound humic substances and humin in the bioavailability of phenanthrene aged in soil. *Environ. Pollut.* **2002**, *118*, 427−433.

(12) Bogan, B. W.; Sullivan, W. R.; Cruz, K. H.; Paterek, J. R.; Ravikovitch, P. I.; Neimark, A. V. "Humic Coverage Index" as a Determining Factor Governing Hydrocarbon Availability to Contaminant-Degrading Bacteria in Soils. *Environ. Sci. Technol.* **2003**, *37*, 5168−5174.

(13) Bogan, B. W.; Sullivan, W. R. Physicochemical soil parameters affecting sequestration and mycobacterial biodegradation of polycyclic aromatic hydrocarbons in soil. *Chemosphere* **2003**, *52*, 1717−1726.

(14) Gregg, S. J.; Sing, K. S. W. *Adsorption, Surface Area and Porosity*; Academic Press: New York, 1982.

(15) Ravikovitch, P. I.; Neimark, A. V. Density functional theory of adsorption in spherical cavities and pore size characterization of templated nanoporous silicas with cubic and three-dimensional hexagonal structures. *Langmuir* **2002**, *18*, 1550−1560.

(16) Neaman, A.; Pelletier, M.; Villieras, F. The effects of exchanged cation, compression, heating and hydration on textural proper-

ties of bulk bentonite and its corresponding purified montmorillonite. *Appl. Clay Sci.* **2003**, *22*, 153−168.
(17) Olivier, J. P.; Occelli, M. L. Surface area and microporosity of a pillared interlayered clay (PILC) from a hybrid density functional theory (DFT) method. *J. Phys. Chem. B* **2001**, *105*, 623−629.
(18) Mayer, L. M. Extent of coverage of mineral surfaces by organic matter in marine sediments. *Geochim. Cosmochim. Acta* **1999**, *63*, 207−215.
(19) Jaroniec, M.; Madey, R. *Physical Adsorption on Heterogeneous Solids*; Elsevier: Amsterdam, 1988.
(20) Villieras, F.; Michot, L. J.; Bardot, F.; Chamerois, M.; Eypert-Blaison, C.; Francois, M.; Gerard, G.; Cases, J. M. Surface heterogeneity of minerals. *C. R. Geosci.* **2002**, *334*, 597−609.
(21) Mayer, L. M. Personal communication.
(22) Arnarson, T. S.; Keil, R. G. Organic-mineral interactions in marine sediments studied using density fractionation and X-ray photoelectron spectroscopy. *Org. Geochem.* **2001**, *32*, 1401−1415.
(23) White, J. C.; Ravikovitch, P. I.; Russo, R.; Neimark, A. V.; Pignatello, J. J. *1996-1998 Bioremediation Research Program Review: EPA/600/R-89/122*; U.S. Environmental Protection Agency: Washington, DC, 1998; pp 19−20.
(24) Vishnyakov, A.; Ravikovitch, P. I.; Neimark, A. V. Molecular level models for CO2 sorption in nanopores. *Langmuir* **1999**, *15*, 8736−8742.
(25) Ravikovitch, P. I.; Vishnyakov, A.; Russo, R.; Neimark, A. V. Unified approach to pore size characterization of microporous carbonaceous materials from N2, Ar, and CO2 adsorption isotherms. *Langmuir* **2000**, *16*, 2311−2320.
(26) deJonge, H.; MittelmeijerHazeleger, M. C. Adsorption of CO2 and n(2) on soil organic matter: Nature of porosity, surface area, and diffusion mechanisms. *Environ. Sci. Technol.* **1996**, *30*, 408−413.
(27) Echeverria, J. C.; Morera, M. T.; Mazkiaran, C.; Garrido, J. J. Characterization of the porous structure of soils: adsorption of nitrogen (77 K) and carbon dioxide (273 K), and mercury porosimetry. *Eur. J. Soil Sci.* **1999**, *50*, 497−503.
(28) de Jonge, H.; de Jonge, L. W.; Mittelmeijer-Hazeleger, M. C. The microporous structure of organic and mineral soil materials. *Soil Sci.* **2000**, *165*, 99−108.
(29) Pignatello, J. J. Soil organic matter as a nanoporous sorbent of organic pollutants. *Adv. Colloid Interface Sci.* **1998**, *77*, 445−467.
(30) Ravikovitch, P. I.; Neimark, A. V. Diffusion-controlled hysteresis. *Adsorption* **2005**, *11*, 265−270.

Received for review October 29, 2004. Revised manuscript received April 6, 2005. Accepted April 6, 2005.

ES048307B